



# Virtual flux based direct power control of shunt active filter

S. Saidi\*, R. Abbassi and S. Chebbi

*LaTICE Laboratory, Higher National Engineering School of Tunis (ENSIT), University of Tunis, 5 Street Taha Hussein Montfleury 1008, Tunisia.*

Received 26 September 2012; received in revised form 18 November 2013; accepted 14 January 2014

## KEYWORDS

Direct Power Control (DPC);  
 Virtual Flux (VF);  
 Switching table;  
 Shunt Active power Filter (SAF);  
 Harmonic currents;  
 Phase locked loop;  
 Self Tuning Filter (STF).

**Abstract.** Active filters are effective solutions to eliminating harmonic pollution and improving reactive power in the presence of nonlinear loads and unbalanced sources. To reduce the disturbances caused by this type of load, we propose, in this paper, a new control strategy of a shunt active filter. Our method aims to improve electrical quantity behavior in steady and dynamic states, while reducing the installing cost of the filter, through eliminating AC line voltage sensors. This is established by Direct Power Control (DPC), based on Virtual Flux (VF) estimation of the electrical network, using a switching function table. Facing disturbances affecting the electrical network, we have integrated a Phase Locked Loop (PLL), and have implemented and tested our new control strategy in a Matlab/Simulink environment. The results obtained show the effectiveness of the active filter control algorithm in eliminating harmonic currents, and shows an improvement in the reactive power injected from nonlinear loads, which has allowed us to confirm the robustness of the proposed strategy.

© 2014 Sharif University of Technology. All rights reserved.

## 1. Introduction

The use of nonlinear loads, such as diode or thyristor rectifiers, which are usually used for electric traction, air conditioning or lighting units made from fluorescent tubes, causes current and voltage distortion. This leads to malfunction of the device connected to the network [1-3]. To overcome problems caused by these loads, such as harmonics and reactive power consumption, several solutions have been proposed [4,5]. To compensate for the negative effects of nonlinear load presences, active power filters are widely used [1,6,7]. Compared to passive filters which have drawbacks, including the design, which requires a thorough knowledge of the electrical network configuration, and the size, which depends on the harmonic spectrum of load and source impedance [8,9], active filters can both neu-

tralize the harmonics of the upstream polluter system and compensate for reactive power and unbalanced loads, thus, improving system efficiency [10-12].

Among active filters, in this paper, we are interested in presenting shunt filters, whose operating principle is to implement a current source for injecting a compensating current in the opposite phase to the harmonic currents generated by the nonlinear loads. Different control strategies have been proposed for these filters [13-15]. The major disadvantage of these strategies is their very slow dynamic response.

This negative point has encouraged us to study the shunt filter, allowing direct power control. This is in order to acquire, if possible, a very high dynamic response [16-18]. Direct Power Control (DPC) has become more widely used over the last few years in grid connected systems, due to its advantage of controlling active and reactive powers directly without any internal current control loop or PWM modulator.

Thus, our control strategy consists of controlling

\*. Corresponding author. Tel.: +216 97 828 970  
 E-mail address: saidi.salem@gmail.com (S. Saidi)

the instantaneous active and reactive power amplitude in order to generate the command moments of the active filter switches to command [19,20]. It consists of calculating the instantaneous power, based on the estimated virtual flux of the electrical network. Then the references of active and reactive power are compared with their estimated values. The differences between the references and the estimated feedback power values are used as inputs for the hysteresis controllers. The digitized output of hysteresis blocks and the sector of virtual flux vector position are considered as inputs for the switching table used to select the optimum voltage vector ensuring the control of the active and reactive powers. Besides, being present for instantaneous power calculation, virtual flux is also used for synchronizing active filter control in the electrical network. The flux is estimated from the currents and estimated supply voltages. These voltages are determined according to the DC-link voltage and the switching states of the converter arms, without the need of two voltage sensors and a pulse width modulation stage.

This paper is organized as follows: It begins with system configuration and analysis of the control algorithm in Section 2. Next, in Section 3, particular attention has been paid to the adopted phase locked loop. Section 4 deals with the DC-link voltage regulation. Section 5 is devoted to a discussion of simulation results and the main improvements of the DPC-VF strategy are highlighted. Finally, Section 6 contains the main conclusions followed by the appendix and references.

### 2. System configuration

The general structure of the active filter connected in parallel to the network (Figure 1), injects disturbed currents in an opposite phase and equal to those

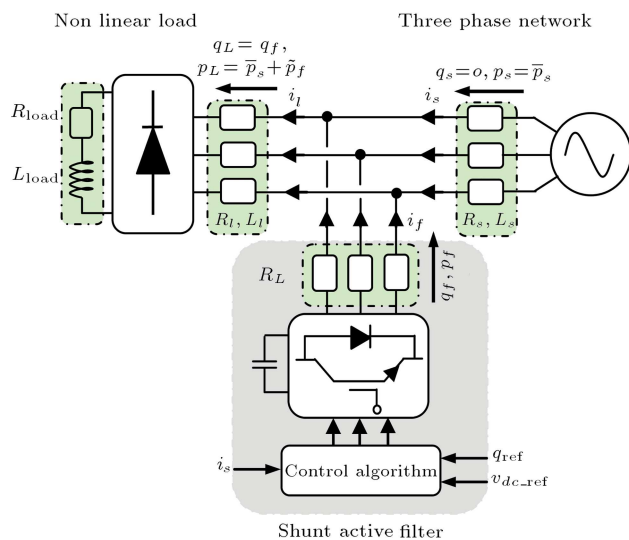


Figure 1. Principle configuration of a shunt APF.

absorbed by the pollutant load. This filter type is used to prevent disturbed currents (harmonic and reactive) circulating through the network impedance located upstream of the connection point of this filter.

In this paper, the active and reactive powers have been considered as state variables. In particular, we recall that power  $p_l$  absorbed by the load is the sum of two components: a DC component,  $\bar{p}_l$ , representing the average value of the load power, and the oscillating component,  $\tilde{p}_l$ :

$$p_l = \bar{p}_l + \tilde{p}_l. \tag{1}$$

In order to compensate for the reactive power and eliminate the harmonic currents, our control strategy operates under the condition in which the electrical grid should only deliver constant instantaneous active power at unity power factor:

$$\begin{cases} p_s = \bar{p}_l \\ q_s = 0 \end{cases} \tag{2}$$

Thus, the power flow is as shown in Figure 2. The total load power ( $p_l$ ) can be provided both by the parallel active filter ( $\tilde{p}_l$ ) and the electrical grid ( $\bar{p}_l$ ), while the reactive power quantity absorbed by the load ( $q_l$ ) must be completely fed by the active filter:

$$\begin{cases} p_f = (p_l - \bar{p}_l) = (\tilde{p}_l) \\ q_f = (q_l - q_s) = (q_l) \end{cases} \tag{3}$$

Energy storage on the DC side is via a capacitive system ( $c_{dc}$ ). The DC link voltage provides the harmonic component of the active power absorbed by the load ( $p_l$ ), which results in compensating for losses in the filter. On the other hand, this supply voltage must provide all of the reactive power absorbed by the non-linear load ( $q_l$ ).

We note that the DC link voltage regulation is important. For this reason, our algorithm assumes that we have a voltage sensor capable of measuring the voltage  $v_{dc}$  (DC link). This measure will be compared to the reference voltage, and a controller, based on a Proportional Integral (PI), treats the error in order to enhance the command performance to maintain the DC link voltage constant and force the injected powers by the filter to follow references estimated by the command.

### 3. Control algorithm

#### 3.1. Principle of direct power control

The basic principle of the DPC was proposed by Noguchi [11] and is similar to the well-known Direct Torque Control (DTC) for induction machines. In the

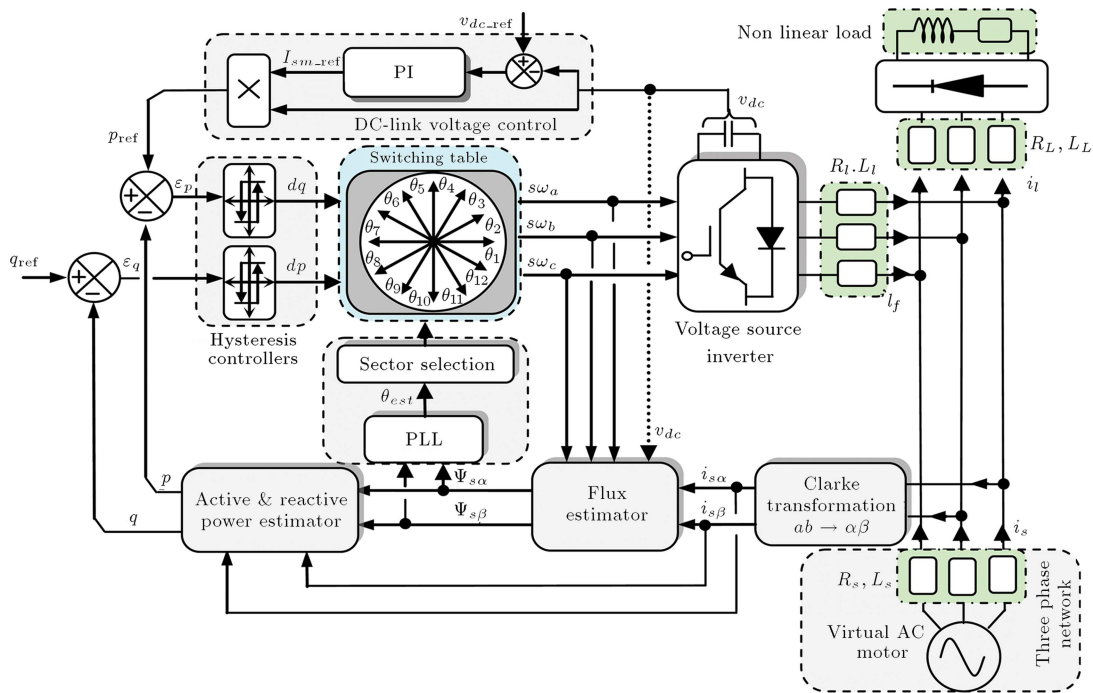


Figure 2. Structure of the command DCP-VF.

DPC, the active and reactive powers replace the torque and the flux amplitude used as the controlled output in the DTC. Figure 2 shows the block diagram of VF-DPC. In this configuration, the active power command,  $p$ , is provided from a DC bus voltage controller block. By fixing the reactive power reference,  $q$ , at zero, the power factor is kept to unity. Therefore, the key point of the VF-DPC implementation is a correct and fast estimation of the active and reactive line powers [15]. The VF-DPC algorithm is based on the assumption that line voltage with input inductances can be noticed as the quantities of a virtual AC motor (Figure 2). The integration of the line voltage gives a virtual flux linkage of a virtual AC motor, based on the measured DC-link voltage,  $v_{dc}$ , and the duty cycle of the modulators,  $sw_a$ ,  $sw_b$  and  $sw_c$ .

Then, the active and reactive power commands ( $p_{ref}$  and  $q_{ref}$ ) are compared with the estimated values of  $p$  and  $q$ . The differences between the commands and the estimated feedback power values,  $\epsilon_p$  and  $\epsilon_q$  ( $\epsilon_p = p_{ref} - p$  and  $\epsilon_q = q_{ref} - q$ ), are entered to the hysteresis controllers. The digitized signal generated by the hysteresis controller of active power, the reactive ( $d_p$  and  $d_q$ ), and the sector of the virtual flux vector position enter the switching table.

The pair of two level hysteresis controllers, as indicated in Figure 2, are used to determine the digitized variables  $d_p$  and  $d_q$ . Independently of the treated variable  $X$  ( $p$  or  $q$ ), the digitized output of the comparator with hysteresis is expressed as follows:

$$dX = 1 \quad \text{if} \quad X \leq X_{ref} - HB_X, \quad (4)$$

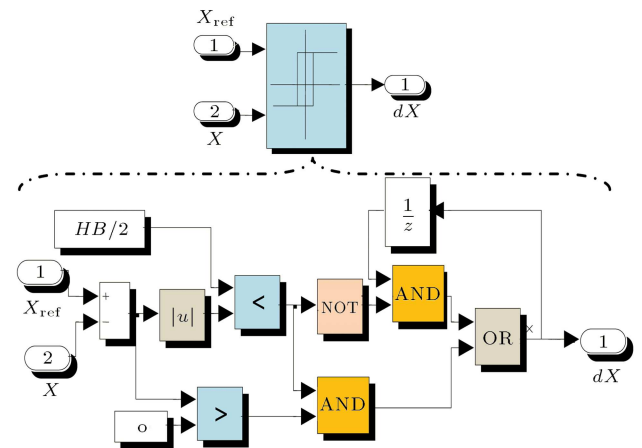


Figure 3. Block diagram of hysteresis control technique.

$$dX = 0 \quad \text{if} \quad X \geq X_{ref} + HB_X, \quad (5)$$

where,  $HB_x$  is the hysteresis bandwidth.

Figure 3 shows the block diagram of the hysteresis comparators. The errors,  $\epsilon_p$  and  $\epsilon_q$  ( $\epsilon_p = p_{ref} - p$  and  $\epsilon_q = q_{ref} - q$ ), are input to the hysteresis comparators and digitized to the signals,  $d_p$  and  $d_q$ . These outputs of both hysteresis controllers are put at state “1” when it is necessary to increase the control variable ( $p$  or  $q$ ), and put at state “0” when this variable must decrease or remain unchanged.

The Boolean variable ( $d_p$  and  $d_q$ ) and the membership sector of the virtual flux vector position form a digital word that accesses the address of lookup table and selects the appropriate voltage vector according to the switching table.

**Table 1.** Switching table for direct power control.

$d_p$	$d_q$	$\theta_1$	$\theta_2$	$\theta_3$	$\theta_4$	$\theta_5$	$\theta_6$	$\theta_7$	$\theta_8$	$\theta_9$	$\theta_{10}$	$\theta_{11}$	$\theta_{12}$
1	0	101	111	100	000	110	111	101	000	011	111	001	000
	1	111	111	000	000	111	111	000	000	111	111	000	000
0	0	101	100	100	110	110	010	010	011	011	001	001	101
	1	100	110	110	010	010	011	011	001	011	101	101	100

With:  $v_1(100)$ ,  $v_2(110)$ ,  $v_3(010)$ ,  $v_4(011)$ ,  $v_5(001)$ ,  $v_6(101)$ ,  $v_0(000)$ ,  $v_7(111)$ .

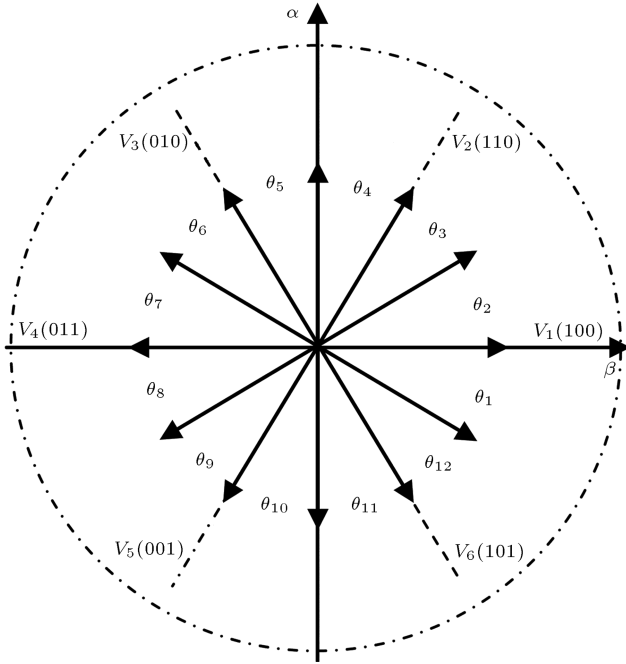


**Figure 4.** Instantaneous voltage vectors.

Herein, each of the control sequences ( $sw_a$ ,  $sw_b$  and  $sw_c$ ) corresponds to a voltage vector,  $v_i$ , at the Shunt Active Filter (SAF) input. Six of them are classified as active vectors, whereas the other two are null vectors. The graphical representation is shown in Figure 4.

The expression of vector,  $v_i$ , in the complex space is defined by the following relationship:

$$v_i = \begin{cases} \sqrt{\frac{2}{3}} \cdot v_{dc} \cdot e^{j(i-1) \cdot \frac{\pi}{3}} & i = \{1, 2, \dots, 6\} \\ 0 & i = \{0, 7\} \end{cases} \quad (6)$$

In order to optimize the SAF input voltage vector and to obtain it as adequate for our purposes, as demonstrated later in the simulation, the region of the flux vector position is divided into 12 sectors of  $30^\circ$ , as shown in Figure 4. The relation between the sectors and the space vector position,  $\theta_n$ , can be expressed as:

$$(n - 2) \cdot \frac{\pi}{6} \leq \theta_n \leq (n - 1) \cdot \frac{\pi}{6} \quad n = \{1, 2, \dots, 12\}. \quad (7)$$

This angle of the line virtual flux vector is given by the

following equation:

$$\theta_n = \tan^{-1} \left( \frac{\Psi_{s\beta}}{\Psi_{s\alpha}} \right). \quad (8)$$

Once the logic outputs of the comparators with hysteresis are established, and, according to the sector number, where vector  $v_i$  is located, the vector of voltages to be applied to the input of the active filter is selected based on the switching (Table 1).

### 3.2. Power estimation based on virtual flux

In order to correctly estimate the power and, at the same time, reduce the number of implemented voltage sensors, Noguchi proposes the use of voltage vector estimation. The implementation of such an approach involves computation of the time derivative of measured currents. The use of a derivative can increase the noise in the control loop, thus, increasing the level of distortion. Recently, the virtual flux strategy was proposed, which assumes basically that the grid voltage and the ac-side inductors are quantities that are related to a virtual motor [13,17].

In accordance with the mentioned control principle, the level measurement of the DC link voltage,  $v_{dc}$ , and the converter switch states,  $sw_a$ ,  $sw_b$  and  $sw_c$ , allow us to express the estimated flux components in  $\alpha$ - $\beta$  reference frame, as follows:

$$\Psi_{s\alpha} = \sqrt{\frac{2}{3}} \cdot v_{dc} \int \left( sw_a - \frac{1}{2}(sw_b + sw_c) \right) \cdot dt + L_s i_{s\alpha}, \quad (9)$$

$$\Psi_{s\beta} = \frac{1}{2} \cdot v_{dc} \int (sw_b - sw_c) \cdot dt + L_s i_{s\beta}. \quad (10)$$

In order to calculate the reference power ( $p_{ref}$ ,  $q_{ref}$ ), from the electrical network currents, in stationary  $\alpha - \beta$  coordinates, and the estimated virtual flux components, we evaluated the voltage in the electrical network by the following equation:

$$\underline{u}_s = R_s \cdot \dot{i}_s + L_s \cdot \frac{d(i_s + \Psi_s)}{dt} = R_s \cdot \dot{i}_s + L_s \cdot \frac{di_s}{dt} + \underline{u}_l. \quad (11)$$

In general, it is assumed that network resistance  $R_s$  is negligible, which allows rewriting Eq. (11) as follows:

$$\underline{u}_s = L_s \cdot \frac{d(i_s + \Psi_s)}{dt} = L_s \cdot \frac{di_s}{dt} + \underline{u}_l. \quad (12)$$

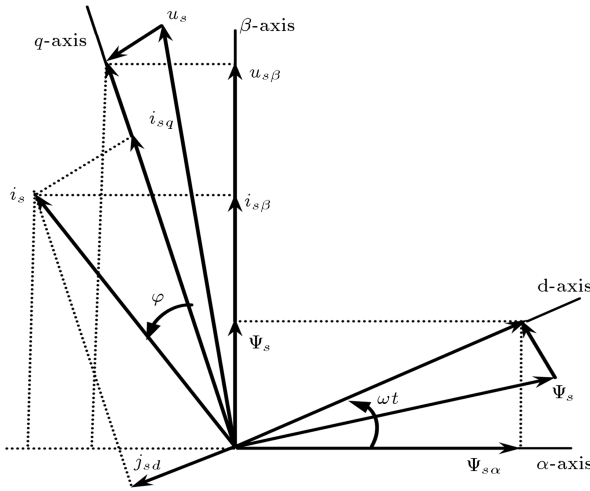


Figure 5. Vector diagram of VF-DPC.

Moreover, the estimated voltage from the virtual flux is expressed as follows:

$$\underline{u}_s = \frac{d}{dt} \underline{\Psi}_s = \frac{d}{dt} (\Psi_s \cdot e^{j\omega t}) = \frac{d\Psi_s}{dt} \cdot e^{j\omega t} + j\omega \cdot \Psi_s \cdot e^{j\omega t} = \frac{d\Psi_s}{dt} \cdot e^{j\omega t} + j\omega \cdot \underline{\Psi}_s \quad (13)$$

In complex notation, the expressions of the instantaneous active and reactive powers are expressed by the following equations:

$$p = \text{Re}(\underline{u}_s \cdot \underline{i}_s^*), \quad (14)$$

$$q = \text{Im}(\underline{u}_s \cdot \underline{i}_s^*), \quad (15)$$

where  $i_s^*$  represent the conjugate of the line current.

In the rotating  $d-q$  reference frame (Figure 5) and for oriented vector control, the instantaneous active and reactive powers are expressed by:

$$p = \frac{d\Psi_{sd}}{dt} \cdot i_{sd} + \omega \cdot \Psi_{sd} \cdot i_{sq}, \quad (16)$$

$$q = -\frac{d\Psi_{sd}}{dt} \cdot i_{sq} + \omega \cdot \Psi_{sd} \cdot i_{sd}. \quad (17)$$

Knowing that  $\frac{d\{\Psi_{sd}\}}{dt}$  is null, then, Expressions (16) and (17) become:

$$p = \omega \cdot \Psi_{sd} \cdot i_{sq}, \quad (18)$$

$$q = \omega \cdot \Psi_{sd} \cdot i_{sd}. \quad (19)$$

As the estimated powers are calculated using the voltages and currents expressed in the stationary reference frame,  $\alpha-\beta$ , clark transformation is essential to reduce the equation number in the new reference frame. This allows rewriting Relation (11) as follows:

$$\underline{u}_s = \left. \frac{d}{dt} \Psi_s \right|_{\alpha} + j \left. \frac{d}{dt} \Psi_s \right|_{\beta} + j\omega \cdot (\Psi_{s\alpha} + j\Psi_{s\beta}). \quad (20)$$

Multiplying the above equation by the current line

vector, we obtain:

$$\underline{u}_s \underline{i}_s^* = \left( \left. \frac{d}{dt} \Psi_s \right|_{\alpha} + j \left. \frac{d}{dt} \Psi_s \right|_{\beta} + j\omega \cdot (\Psi_{s\alpha} + j\Psi_{s\beta}) \right) \cdot (i_{s\alpha} - j i_{s\beta}). \quad (21)$$

Taking into account Expressions 21, Expressions 14 and 15 become:

$$p = \left( \left. \frac{d}{dt} \Psi_s \right|_{\alpha} \cdot i_{s\alpha} + \left. \frac{d}{dt} \Psi_s \right|_{\beta} \cdot i_{s\beta} + \omega \cdot (\Psi_{s\alpha} \cdot i_{s\beta} - \Psi_{s\beta} \cdot i_{s\alpha}) \right), \quad (22)$$

$$q = \left( -\left. \frac{d}{dt} \Psi_s \right|_{\alpha} \cdot i_{s\beta} + \left. \frac{d}{dt} \Psi_s \right|_{\beta} \cdot i_{s\alpha} + \omega \cdot (\Psi_{s\alpha} \cdot i_{s\alpha} + \Psi_{s\beta} \cdot i_{s\beta}) \right). \quad (23)$$

In addition, for a balanced voltage system, the flux amplitude derivative is zero. Thus, the instantaneous active and reactive power becomes:

$$p = \omega \cdot (\Psi_{s\alpha} \cdot i_{s\beta} - \Psi_{s\beta} \cdot i_{s\alpha}), \quad (24)$$

$$q = \omega \cdot (\Psi_{s\alpha} \cdot i_{s\alpha} + \Psi_{s\beta} \cdot i_{s\beta}). \quad (25)$$

To make the command more robust, a phase locked loop (PLL Phase Locked Loop) could be added to recreate a supply voltage without distortion. However, we should seriously consider the impact of this loop on area detection.

### 3.3. Structure of the phase locked loop

The active filter is connected to an active power network. For this reason, the fundamental frequency of the inverter output voltage has to be the same as the network frequency, which is not always constant and equal to 50 Hz. Moreover, it is necessary to know the phase displacement of the network voltage in order to apply the inverter voltage with the correct phase shift. An algorithm capable of detecting both the frequency and the phase displacement of the network voltage is therefore needed. Such an algorithm has been implemented, making use of a Phase-Locked Loop algorithm (PLL).

Hence, the PLL principle (Figure 6) is based on the extraction of fundamental components,  $\Psi_{sf\alpha}$  and  $\Psi_{sf\beta}$ , from components  $\Psi_{s\alpha}$  and  $\Psi_{s\beta}$  of the virtual flux. Based on the filtered values, the values of  $\sin(\theta_{est})$  and  $\cos(\theta_{est})$  are deduced.

The Self-Tuning Filter (STF) was developed by M. Benhabibe [15]. It is based on the work of Song

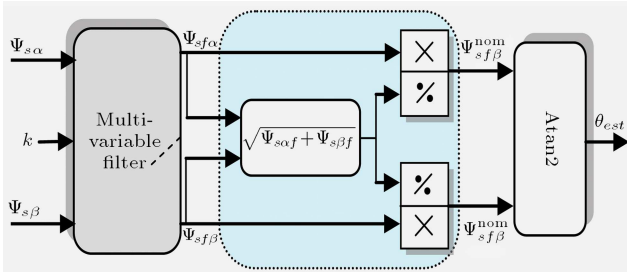


Figure 6. Basic block diagram of the vector PLL system.

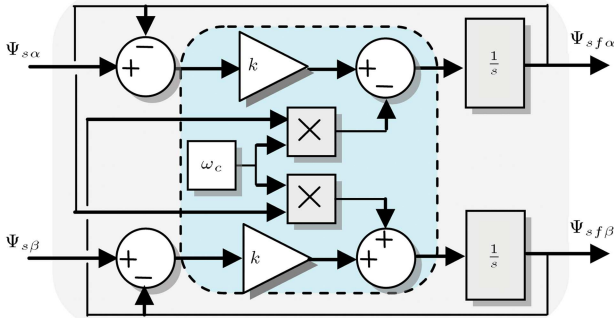


Figure 7. The extraction of fundamental virtual flux components via STF.

Hong-Skok, which is based on the extraction of fundamental signals directly from the  $\alpha$ - $\beta$  axes. However, it allows the extraction of fundamental components of the estimated flux. The transfer function of this STF is expressed by the following equation:

$$\frac{\Psi_{s\alpha\beta f}(s)}{\Psi_{s\alpha\beta}(s)} = k \frac{(s+k) + j\omega_c}{(s+k)^2 + \omega_c^2}, \quad (26)$$

where  $\Psi_{s\alpha\beta}$  and  $\Psi_{s\alpha\beta f}$  are the instantaneous signals, respectively, before and after integration in the SRF, and  $k$  is the constant gain.

By developing this equation, we obtain the expressions:

$$\Psi_{sf\alpha}(s) = \frac{k}{s} \cdot (\Psi_{s\alpha}(s) - \Psi_{sf\alpha}(s)) - \frac{\omega_c}{s} \cdot \Psi_{s\beta f}(s), \quad (27)$$

$$\Psi_{sf\beta}(s) = \frac{k}{s} \cdot (\Psi_{s\beta}(s) - \Psi_{sf\beta}(s)) + \frac{\omega_c}{s} \cdot \Psi_{s\alpha f}(s). \quad (28)$$

The block diagram of this STF is illustrated in Figure 7.

According to the value of “ $k$ ”, STF selectivity is possible (Figure 8). Indeed, we note that pulsation  $\omega = \omega_c$ , and that, for all curves, the phase shift introduced by the STF, is zero and the gain is unitary. Moreover, we remarked that the decrease of the  $k$  value increases STF selectivity. Thus, using a STF, the fundamental and harmonic direct or inverse components of input signals are taken directly along the  $\alpha$ - $\beta$  axes, without phase shift or amplitude change.

In order to test the PLL effectiveness, we simulated the phase jump case,  $-\pi/2$ , of the network voltage. The result (Figure 9) shows that the response is

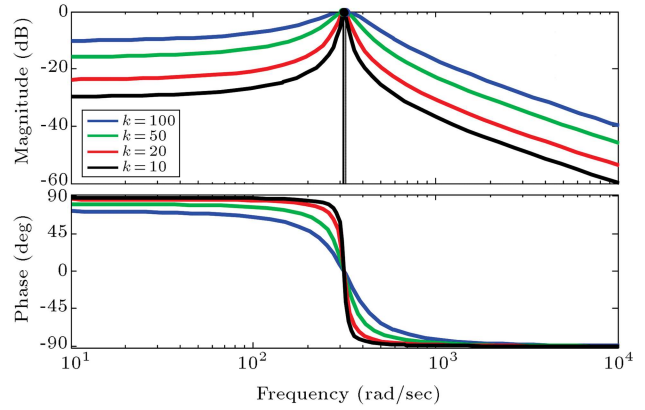


Figure 8. Bode diagram for the STF for different values of the parameter  $k$ .

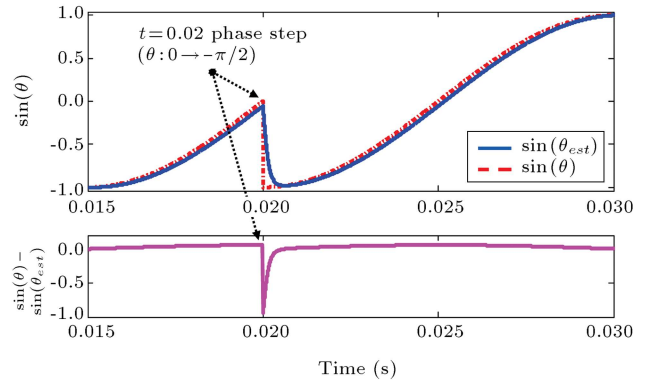


Figure 9. Self-tuning filter response ( $k = 100$ ).

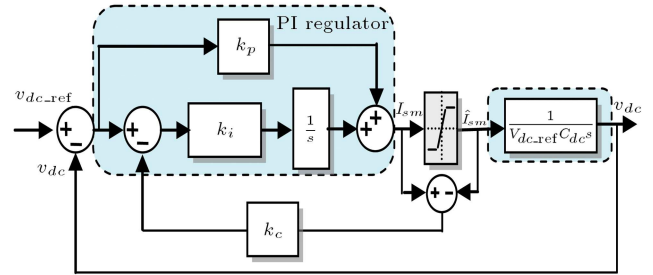


Figure 10. Anti-windup PI controller.

much better, which proves that the proposed analytical approach for the design of a multi-variable filter is quite rigorous. A gap in transient mode, relatively small, is visible on a zoom at the time of the variation.

For a normal operating condition, the power active filter requires maintaining the voltage across the condenser at a constant value.

### 3.4. DC bus current balance control

In order to limit supply voltage fluctuations of the active filter and not decrease the filtering performance, a proportional-integral corrector (Figure 10) is used. Following the variation between the measured value ( $v_{dc}$ ) and the reference value ( $v_{dc\_ref}$ ), the output loop becomes an estimation of the maximum current from

the source ( $I_{sm}$ ). This current is used to calculate the reference power ( $p_{ref}$ ) requested by the active filter and the losses caused by the power active filter.

Taking into account the PI regulator transfer function and that of the DC side, the transfer function of the control loop is:

$$\begin{aligned} \frac{v_{dc}}{v_{dc\_ref}} &= \frac{3v_s^2(1 + \tau_n \cdot s)}{(v_{sm} \cdot c_{dc} \cdot \tau_i \cdot v_{dc\_ref})s^2 + (3\tau_n \cdot v_s^2) \cdot s + 3v_s^2} \\ &= \frac{3v_s^2(1 + \tau_n \cdot s)}{v_{sm} \cdot c_{dc} \cdot \tau_i \cdot v_{dc\_ref} s^2 + 2\xi\omega_c \cdot s + \omega_c^2}, \end{aligned} \quad (29)$$

with,  $\omega_c$ , the cutoff frequency, expressed by:

$$\omega_c = \sqrt{\frac{3v_s^2}{v_{sm} \cdot c_{dc} \cdot \tau_i \cdot v_{dc\_ref}}}, \quad (30)$$

and,  $\xi$ , the damping coefficient, given by:

$$\xi = \frac{3\tau_n \cdot v_s^2}{2\omega_c \cdot v_{sm} \cdot c_{dc} \cdot \tau_i \cdot v_{dc\_ref}} = \frac{\sqrt{3}\tau_n \cdot v_s}{2\sqrt{v_{sm} \cdot c_{dc} \cdot \tau_i \cdot v_{dc\_ref}}}. \quad (31)$$

This function can be set as follows:

$$\frac{v_{dc}}{v_{dc\_ref}} = \frac{\omega_c^2 + (2 \cdot \omega_c \cdot \xi \cdot \tau_n) \cdot s}{s^2 + 2\xi\omega_c \cdot s + \omega_c^2}. \quad (32)$$

In order to realize a good trade-off between stability and dynamic performance, one can choose  $\xi = 0.7$  and  $\omega_c = 2\pi f_c$ . Finally, we deduce the time constants  $\tau_i$  and  $\tau_n$ :

$$\begin{cases} \tau_i = \frac{3v_s^2}{v_{sm} \cdot c_{dc} \cdot \omega_c^2 \cdot v_{dc\_ref}} \\ \tau_n = \frac{2\xi \cdot \sqrt{v_{sm} \cdot c_{dc} \cdot \tau_i \cdot v_{dc\_ref}}}{\sqrt{3} \cdot v_s} \end{cases} \quad (33)$$

where:

- $\xi$  is the damping coefficient and  $\omega_c$  is the cut-off frequency;
- $k_p$ ,  $k_i$ ,  $\tau_i$  and  $\tau_n$  are the proportional constant, the integral constant, the integration time constant and the time constant of the PI controller, respectively.

It is important to note that the calculation of the integral component takes into account the limitation on the order;

- If error ( $v_{dc\_ref} - v_{dc}$ ) is positive for a certain period of time, control signal  $\hat{I}_{sm}$  saturates to the maximum value,  $I_{sm}$ ;
- If the error remains positive after the saturation of  $\hat{I}_{sm}$ , the integrator continues to accumulate an error that will be difficult to cancel in a reasonable period of time. This can causes a significant error in output, and even system instability.

To avoid this effect, we have added a loop using a new error signal defined as the difference between the controller output,  $I_{sm}$ , and the actuator output,  $\hat{I}_{sm}$ , weighted by a gain,  $k_c$ .

#### 4. Simulation results

The first scenario is to analyze network behavior in the presence of a load quantity assumed as a total amount. The second scenario focuses on network behavior in case of a load increase and a partial loss of load. The studied system parameters are summarized in Table 2 and simulated using a “Power System Blockset” and “Simulink” under a Matlab environment.

Table 2. Simulation parameters.

Parameters	Symbol	Value
<b>Electrical network</b>	Source voltages	$v_s$ 220 V
	Source resistor	$R_s$ 0.5 $\Omega$
	Source inductor	$L_s$ 5 $\mu$ H
	Source frequency	$f$ 50 Hz
<b>Nonlinear load</b>	Load resistor	$R_{load}$ 9 $\Omega$ or 7 $\Omega$
	Load inductor	$L_{load}$ 1 mH
<b>Active power filter</b>	DC-bus capacitor	$c_{dc}$ 1600 $\mu$ F
	Interfacing inductor	$R_L$ 0.7 mH
	Interfacing resistor	$L_L$ 0.01 $\Omega$
	Switching frequency	$F$ 20 kHz
<b>Serie load filter and hysteresis tolerance band</b>	Resistance	$R$ 0.01 $\Omega$
	Inductance	$L_l$ 50 $\mu$ H
	Hysteresis band	$HB_X$ 0.01
<b>Coefficients of the PI</b>	Proportional constant	$K_p$ 0.22
	Integral constant	$k_i$ 76.2

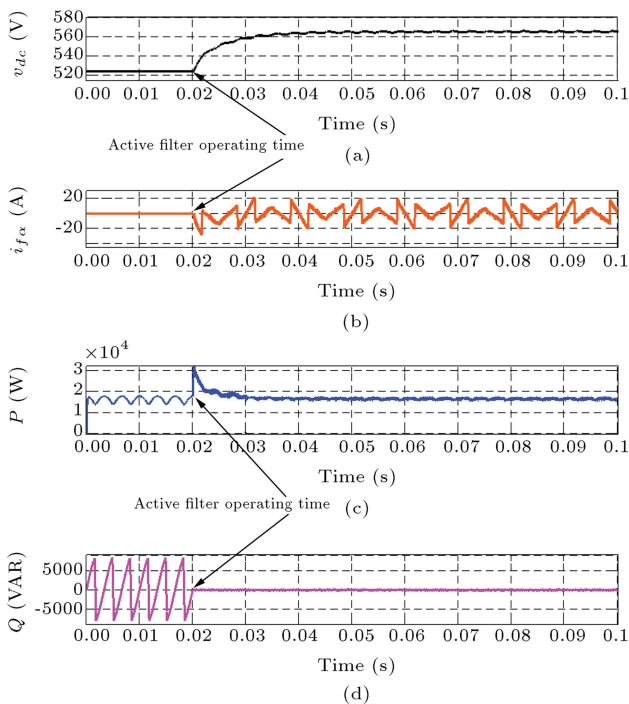


**Figure 11.** (a) DC side capacitor voltage, (b) filters current waveforms, and (c) instantaneous active powers waveforms at the source side.

#### 4.1. First scenario

In the presence of a nonlinear load in the Graëtz bridge with six diodes connected to a three-phase network, as shown in Figure 1, we simulated network behavior following the insertion of a parallel active filter at time  $t = 0.02$  s.

The results show that after the integration of the proposed parallel active filter, the DC-link bus voltage (Figure 11(a)) reaches its reference value imposed by the control algorithm. Furthermore, we note that, even with low ripple, the answer is better, thanks to the use of the twelve sectors table. Moreover, we note that the reactive power and harmonic component of active power (Figure 11(c) and (d)) are zero, confirming the unity of the power factor.

Furthermore, the results show an improvement in network current waveform (Figure 12(a)). This current has filtered at a satisfactory level. Hence, there is an improvement of power factor, since current ( $i_{sa}$ ) and voltage ( $v_{sa}$ ) are perfectly in phase (Figure 12(b)). The fact that  $i_{sa}$  was able to recover the waveform, confirms that the active filter has generated a harmonic current ( $i_{fa}$ ) (Figure 11(b)) of the same amplitude, but in an opposite phase to that absorbed by the nonlinear load.

Following the spectral analysis of one network phase current, before and after integration of the active filter, Figure 13(a) shows the symmetrical distortion of current  $i_{sa}$ . This means that only harmonics of the  $(6h \pm 1)$ th order are present. This is confirmed

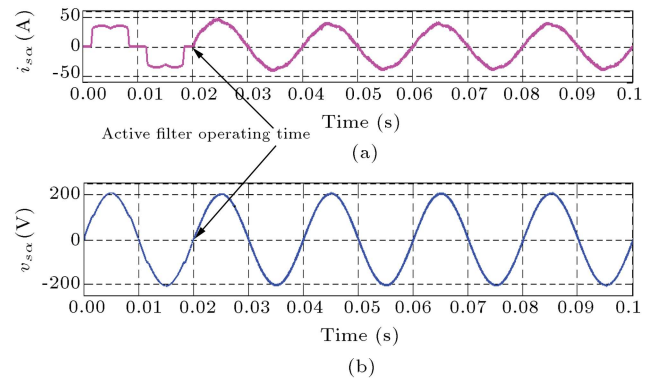


**Figure 12.** (a) Source phase current waveforms. (b) Voltage waveform.

by the spectrum  $i_{sa}$  (Figure 13(b)), which shows the importance of the 5th and 7th order harmonics.

On the other hand, we show that after filter insertion, the current waveform is sinusoidal (Figure 14(a)) and there are virtually no harmonics (Figure 14(b)). In the absence of filtering, the harmonic ratio is 30.13%, whereas, in the presence of active filtering, this rate is reduced to 0.92%, which is well below the permissible limit of 5%, as required by the norm of the International Electrotechnical Commission (IEC).

To observe the effectiveness of the proposed strategy, we followed the temporal evolution of flux variables provided by direct power control (Figure 15(a)). It is noted that the two flux components  $\Psi_{s\alpha}$  and  $\Psi_{s\beta}$  are in quadrature, and perfectly sinusoidal which is correlated with Figure 16 where a quasi-circular trajectory describes the end of the flux vector  $\Psi_{s'}$ , in the stationary frame ( $\alpha - \beta$ ). The network angles ( $\theta_{est}$  and  $\theta$ ) (Figure 15(b)), have a periodic saw tooth curve and a better response of the PLL.

The wave form of the output voltage of the active filter ( $v_{an}$ ) and those of control signals,  $s_{wa}$  and  $\overline{sw}_a$  show that the two voltage levels  $v_{dc}/3$  and  $2v_{dc}/3$  appear clearly and correspond respectively to 188 V and 376 V consistent with the voltage taken as a reference (Figure 17). These results prove the effectiveness of our strategy.

#### 4.2. Second scenario

This scenario assumes that from an established operating system, a new call of power takes place at time  $t = 0.2$  s; this is an increase in resistance ( $R_{load} = 9 \Omega$ ). From the new equilibrium state, we assume that at time  $t = 0.26$  s, there was a decrease in resistance ( $R_{load} = 7 \Omega$ ). For this case, we simulated voltage level temporal evolutions and those of active and reactive power.

Figures 18 and 19 show the obtained simulation results. We note that changes in load cause a change in the consumed current and, therefore, in the instantaneous active power reference. Our direct power control came to respond very quickly to a change in the power

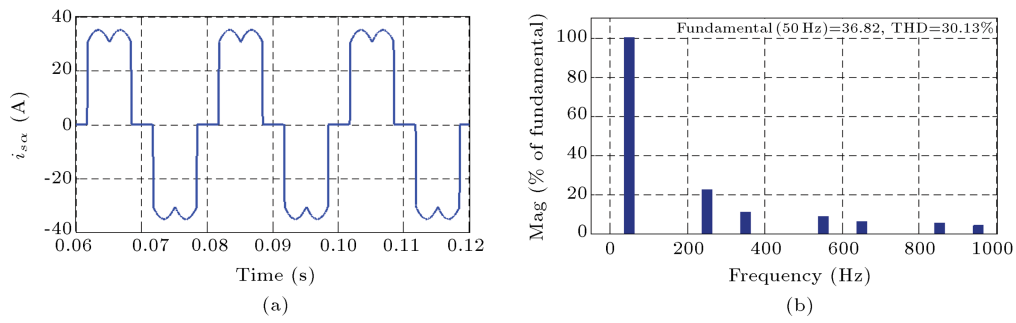


**Figure 13.** (a) Curve before active filtering. (b) Spectral analysis of the current before active filtering.

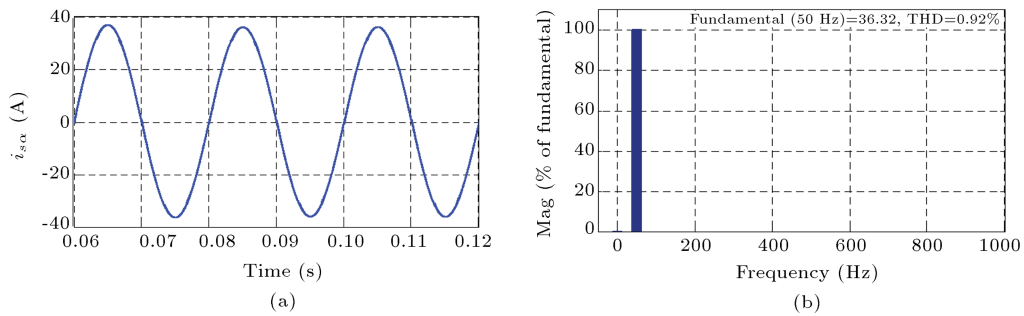


**Figure 14.** (a) Curve after active filtering. (b) Spectral analysis of the current after active filtering.

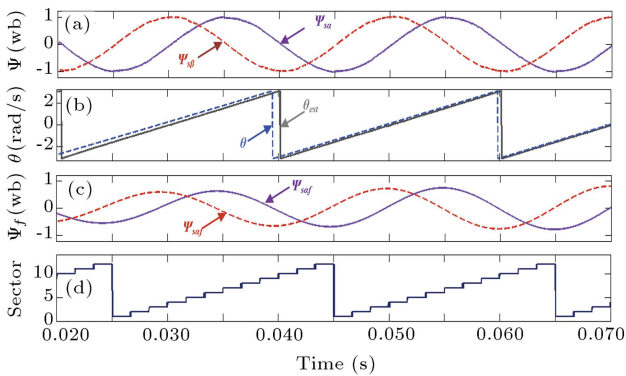


**Figure 15.** (a) Flux components. (b) Electrical angle. (c) Flux components estimated. (d) Instant location of sectors  $\Psi_s$ .

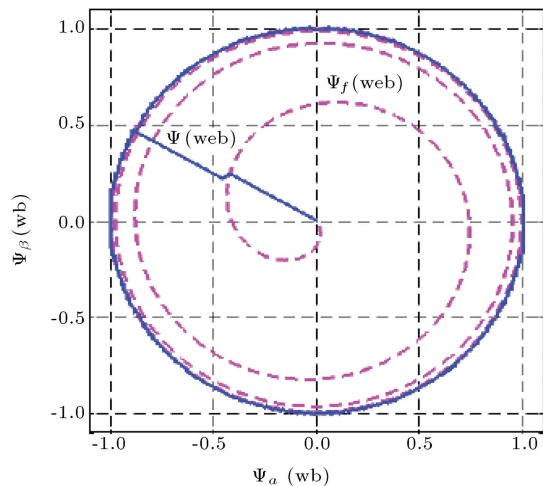


**Figure 16.** The end flux vector trajectory.

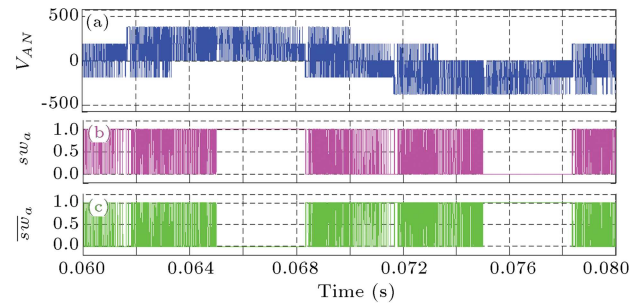


**Figure 17.** (a) Output voltage of active filter. (b) and (c) Control signals.

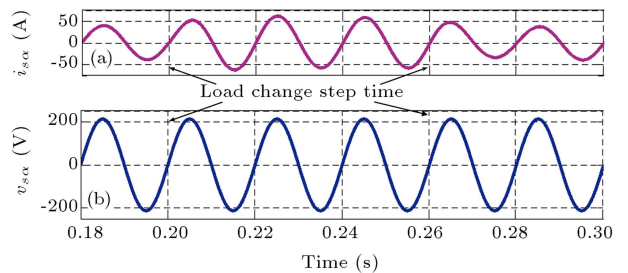


**Figure 18.** (a) Source phase current waveforms. (b) Voltage waveform.

set point. We also notice a ripple superimposed on the DC-link voltage whose origin is attributed to the network voltage distortion.

### 5. Conclusion

In this paper, we studied a new control strategy, which derives from the direct power control flow through

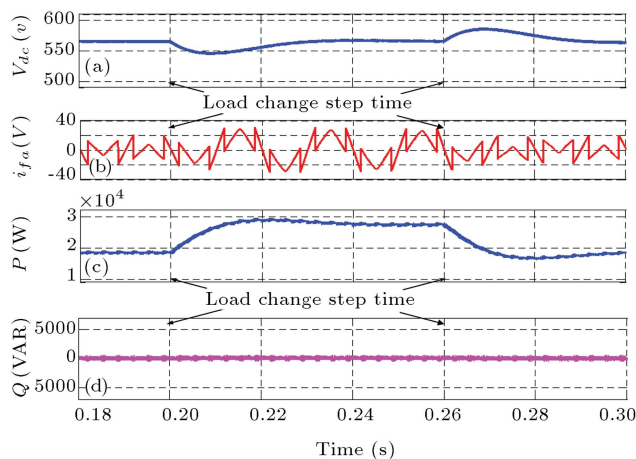


**Figure 19.** (a) DC side capacitor voltage filters. (b) Current waveforms. (c) Instantaneous active powers waveforms at the source side. (d) Instantaneous reactive powers waveforms at the source side.

the virtual network. This strategy is formulated for an active filter connected in parallel to a network in order to inject currents, eliminating harmonics caused by the presence of nonlinear loads. Our strategy has advantages compared to the voltage estimation method and, therefore, it allows working with a smaller sampling frequency and providing better performance when the network voltage is disturbed. Thus, this method is simple and effective. In addition, it has better performance in terms of current harmonics compensations, power factor and performances in steady and dynamic states. Our strategy on one hand allowed us to mitigate the harmonic rate of the network side (THD) and provide sinusoidal line currents. On the other hand, it has reduced the cost of installation of our active filter.

## Nomenclature

$p_s$ and $q_s$	Instantaneous active and reactive power of sources
$p_f$ and $q_f$	Instantaneous active and reactive power of shunt active filter
$p_l$ and $q_l$	Instantaneous active and reactive power absorbed by nonlinear loads
$R_s$ and $L_s$	Resistor and inductor of filter network
$R_l$ and $L_l$	Resistor and inductor of series load
$R_{load}$ and $L_{load}$	Resistor and inductor of connection nonlinear loads
$R_L$ and $L_L$	Resistor and inductor of connection filter
$v_{dc}$	DC bus voltage
$c_{dc}$	Flying capacitor
$sw_i$	Switching signals, $i \in [a, b, c]$
$\Psi$	Modulus of virtual flux vector

$\underline{\Psi}_s$	Virtual flux vector
$\underline{u}_s$	Voltage vector
$\underline{i}_s$	Line current vector
$\omega$	Cut off pulse filter
$k$	Positive constant
$v_s$	Voltage of power source

## References

1. Akagi, H. "Control strategy of active power filters using multiple voltage-source PWM converters", *IEEE Trans. on Industrial Applications*, **22**(3), pp. 460-465 (1986).
2. Akagi, H. "Active harmonic filters", *Proceedings of the IEEE*, **93**(12), pp. 2128-2141 (2005).
3. Saidi, S., Chebbi, S. and Jouini, H. "Harmonic and reactive power compensations by shunt active filter controlled by adaptive fuzzy logic", *International Review of Electrical Engineering*, **4**(4), pp. 1487-1492 (2011).
4. Chaoui, A., Gaubert, J.P. and Krim, F. "Power quality improvement using DPC controlled three-phase shunt active filter", *Electric Power Systems Research*, **80**(6), pp. 657-666 (2010).
5. Kazmierkowski, M.P. and Malesani, L. "Current control techniques for three-phase voltage-source PWM converters, A survey", *IEEE Trans. Ind. Electronics*, **45**, pp. 691-703 (1998).
6. Zhang, H., Merhr, A.S. and Shi, Y. "Improved robust energy-to-peak filtering for uncertain linear systems", *Signal Processing*, **90**(9), pp. 2667-2675 (2010).
7. Singh, B., Al-Haddad, K. and Chandra, A. "A review of active filters for power quality improvement", *IEEE Trans. Ind. Electronics*, **46**(5), pp. 960-971 (1999).
8. Bouafia, A., Gaubert, J.P. and Krim, F. "Design and implementation of predictive current control of three-phase PWM rectifier using space-vector modulation (SVM)", *Energy Conversion and Management*, **50**(1), pp. 6-13 (2009).
9. Lou, Z.E. and Gao, Y. "The exponential stability for a class of hybrid systems", *Asian Journal of Control*, **15**(2), pp. 624-629 (2013).
10. Zhang, H., Merhr, A.S. and Shi, Y. "Robust weighted H infinity filtering for networked systems with intermittent measurements of multiple sensors", *International Journal of Adaptive Control and Signal Processing*, **25**(4), pp. 313-330 (2011).
11. Monfared, M., Rastegar, H. and Kojabadi, H.M. "High performance direct instantaneous power control of PWM rectifiers", *Energy Conversion and Management*, **51**(5), pp. 947-954 (2010).

12. Zhang, H., Merhr, A.S. and Shi, Y. "On H<sub>∞</sub> filtering for discrete-time Takagi-Sugeno fuzzy systems", *IEEE Trans. Fuzzy Systems*, **20**(2), pp. 396-401 (2012).
13. Malinowski, M., Kazmierkowski, M.P., Hansen, S., Blaabjerg, F. and Marques, G.D. "Virtual-flux-based direct power control of three-phase PWM rectifiers", *IEEE Trans. Ind. Applications*, **37**(4), pp. 1019-1027 (2001).
14. Omeiri, A., Haddouche, A., Zellouma, L. and Saad, S. "A three-phase shunt active power filter for currents harmonics suppression and reactive power compensation", *Asian Journal of Information Technology*, **5**(12), pp. 1454-1457 (2006).
15. Abdusalam, M., Poure, P., Karimi, S. and Saadate, S. "New digital reference current generation for shunt active power filter under distorted voltage conditions", *Electric Power Systems Research*, **79**(5), pp. 759-765 (2009).
16. Wang, D.J. and Gao, X.L. "Stability margins and H<sub>∞</sub> co-design with fractional-order PID controllers", *Asian Journal of Control*, **15**(3), pp. 691-697 (2013).
17. Noguchi, T., Tomiki, H., Kondo, S. and Takahashi, I. "Direct power control of PWM converter without power-source voltage sensors", *IEEE Trans. Ind. Applications*, **34**(3), pp. 473-479 (1998).
18. Hyosung, K., Blaabjerg, F., Bak-Jensen, B. and Jaeho, C. "Instantaneous power compensation in three-phase systems by using p-q-r theory", *IEEE Transaction on Power Electronics*, **17**(5), pp. 701-710 (2002).
19. Sato, A. and Noguchi, T. "Voltage-source PWM rectifier-inverter based on direct power control and its

operation characteristics", *IEEE Trans. Ind. Power Electronics*, **26**(5), pp. 1559- 1567 (2011).

20. Zhang, H., Merhr, A.S. and Shi, Y. "Robust energy-to-peak filtering for networked systems with time-varying delays and randomly missing data", *IET Control Theory & Applications*, **4**(12), pp. 2921-2936 (2010).

### Appendix

$R_s$  and  $L_s$  represent the stator resistance and the stator leakage inductance of the virtual motor and phase-to-phase line voltages;  $u_{ab}$ ,  $u_{bc}$  and  $u_{ca}$  would be induced by a virtual air-gap flux. In other words, the integration of the phase-to-phase voltages leads to a virtual line flux vector,  $\underline{\Psi}_s$ , in stationary  $\alpha$ - $\beta$  coordinates. With the definitions:

$$\underline{\Psi}_s = \begin{pmatrix} \Psi_{s\alpha} \\ \Psi_{s\beta} \end{pmatrix} = \begin{pmatrix} \int u_{s\alpha} \cdot dt \\ \int u_{s\beta} \cdot dt \end{pmatrix},$$

where:

$$\underline{u}_s = \begin{pmatrix} u_{s\alpha} \\ u_{s\beta} \end{pmatrix} = \sqrt{2/3} \begin{pmatrix} 1 & 1/2 \\ 0 & \sqrt{3}/2 \end{pmatrix} \begin{pmatrix} u_{ab} \\ u_{bc} \end{pmatrix},$$

$$\underline{i}_s = \begin{pmatrix} i_{s\alpha} \\ i_{s\beta} \end{pmatrix} = \sqrt{2/3} \begin{pmatrix} 3/2 & 0 \\ \sqrt{3}/2 & \sqrt{3} \end{pmatrix} \begin{pmatrix} i_{sa} \\ i_{sb} \end{pmatrix},$$

$$\underline{u}_L = \begin{pmatrix} u_{L\alpha} \\ u_{L\beta} \end{pmatrix} = \sqrt{2/3} \begin{pmatrix} 1 & -1/2 & -1/2 \\ 0 & \sqrt{3}/2 & -\sqrt{3}/2 \end{pmatrix} \begin{pmatrix} u_{AM} \\ u_{BM} \\ u_{CM} \end{pmatrix}.$$

The block diagram of the proposed control strategy is depicted in Figure A.1 and the simulation parameters are grouped in Table 2.

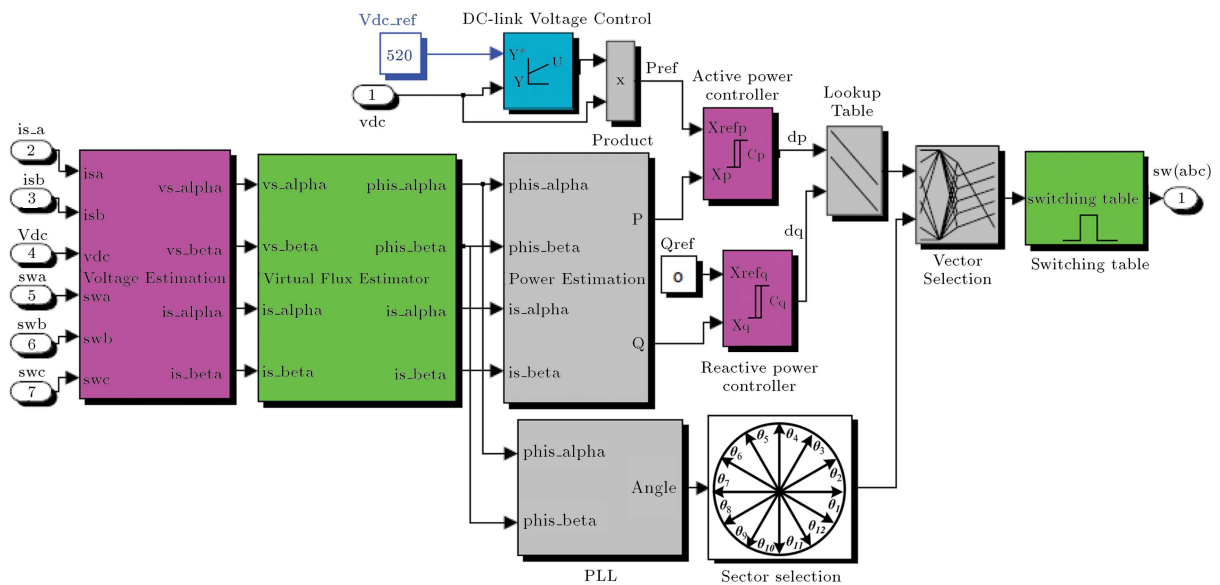


Figure A.1. DPC-VF block diagram.

## Biographies

**Salem Saidi** received the MS degree in Electrical Engineering from Higher National Engineering School of Tunis - Tunisia (ENSIT), Tunis University, in 2009. Currently, he is preparing a PhD degree thesis on electrical networks and active power filtering in the LaTICE laboratory. He is interested in power electronics and machine modeling, control induction Motor drives, Pulse Width Modulation, Multilevel inverter and active filter.

**Rabeh Abbassi** received the PhD degree in electrical engineering from the Higher National Engineering School of Tunis (ENSIT), Tunis University, Tunisia, in

2014. Since 2007, he has been with LaTICE laboratory. His research interests include renewable energies, smart grid, wind turbines control, photovoltaic systems, storage systems, integration of distributed generation, control of power converters and power conditioning. He is also an Assistant Professor with the Department of Electrical Engineering at ISSATK.

**Souad Chebbi** obtained her PhD degree in 1983 in Electrical Engineering. She is head of the Laboratory of Technologies of Information and Communication and Electrical Engineering (LaTICE), at the Higher National Engineering School of Tunis (ENSIT), University of Tunisia. Her research is in the areas of electrical networks and electrical systems.